AGU100 ADVANCING EARTH AND SPACE SCIENCE

Radio Science

RESEARCH ARTICLE

10.1029/2018RS006671

Key Points:

- Surface refractivity and its gradient were calculated using collected local meteorological data for a period of 35 years in the lowest atmospheric layer above the ground
- The evolution of the surface refractivity has two cycles; in one cycle, the evolution depends mainly on the inverse of the temperature; in the second cycle, this evolution depends mainly on the water vapor pressure, that is, humidity
- The results of the analysis show that the linear trends of the yearly variations of the vertical refractivity gradient over the analyzed period decay from year to year; such a trend may increase the occurrence of superrefraction; note that this observation is based on the estimated values of dN_1; in the future, we hope that the measured values of local meteorological data will be available

Supporting Information:

- Supporting Information S1

Correspondence to:
H. Obeidat,
h.obeidat@jpu.edu.jo

Citation:
Bettouche, Y., Kouki, A., Agba, B., Obeidat, H., Alhassan, H., Rodriguez, J., et al. (2019). Long-term evolution of the surface refractivity for Arctic regions. *Radio Science*, *54*, 602–611. https://doi.org/10.1029/2018RS006671

Received 18 JUN 2018
Accepted 22 JUN 2019
Accepted article online 2 JUL 2019
Published online 19 JUL 2019

Long-Term Evolution of The Surface Refractivity for Arctic Regions

Y. Bettouche[1], H. Obeidat[2], B. Agba[1], A. Kouki[1], H. Alhassan[3], Jonathan Rodriguez[4], R. Abd-Alhameed[3], and S. Jones[3]

[1]École de Technologie Supérieure, Montréal, Canada, [2]Faculty of Engineering, Jerash University, Jerash, Jordan, [3]Faculty of Engineering and Informatics, University of Bradford, Bradford, UK, [4]Instituto de Telecomunicações, Campus Universitário de Santiago, Aveiro, Portugal

Abstract In this paper, local meteorological data for a period of 35 years (from 1979 to 2013) from Kuujuaq station have been used to calculate the surface refractivity, N (a link for the data is available in the acknowledgements), and to estimate the vertical refractivity gradient, dN_1, in the lowest atmospheric layer above the ground. Monthly and yearly variations of the mean of N and dN_1 are provided. The values obtained are compared with the corresponding values from the ITU maps. The long-term trend of the surface refractivity is also investigated. The data demonstrate that the indices N and dN_1 are subject to an evolution that may have significance in the context of climate change. Monthly means of N show an increasing departure from ITU-R values since 1990. Yearly mean values of the dN_1 show a progressive decrease over the period of study. Seasonal means of dN_1 show a decrease over time, especially for summer. Such a trend may increase the occurrence of superrefraction. However, currently available ITU-R recommendations for microwave link design assume a stationary climate, so there is a need for a new modeling approach.

1. Introduction

This paper addresses issues in the design of terrestrial microwave links in Arctic regions that arise in the context of climate change (*CC*). The study was motivated when the impact of an exceptional ice storm in the Montreal region on electrical installations demonstrated the vulnerability of public and commercial infrastructure to climate hazards (R-3670-2008, D, 2009). After the ice storm, the telecommunications team of regional electricity generation and distribution company, Hydro-Québec TransEnergie (HQ), recommended that in addition to fiber optic links, microwave links are to be used in order to ensure continuity of service under normal, as well as in catastrophic conditions (R-3670-2008, D, 2009). As a company involved in the transmission and distribution of electricity, HQ questioned whether CC would have an impact on the design methods for their microwave links.

Since 2008, HQ has used the ITU-R P.530 Recommendations (Recommendations, I, 2017) for the design of terrestrial links. They provided a method for calculating the incidence of narrow band fading due to multipath propagation for small percentages of time at a given frequency anywhere on Earth.

It is well known that when radio waves propagate through a stratified atmosphere, refraction takes place. In an ITU-R Standard Atmosphere, the refractive index of air $n(h)$ decreases exponentially with height h in kilometers, causing rays to bend toward the Earth, thus extending the radio horizon. Nonstandard refraction of radio waves can lead to significant variation in received power level (Ali et al., 2012; Zilinskas et al., 2012) for both intended and unintended receivers. To obtain reliable communication links, several criteria, such as antenna heights and gains, power levels, path profile, distance, geographical location, and atmospheric conditions and properties must be considered in the design/planning phase.

The radio refractivity, N, measured in N units (Freeman, 2006; Guo & Li, 2000; related to n, see equation (2)) depends on the meteorological parameters, particularly temperature, humidity, and partial water vapor pressure. Since these parameters vary with height, the refractivity will also vary with height and will, therefore, have a gradient dN/dh. Values of meteorological parameters are used to estimate the values of the refractivity and the refractivity gradient. Even small changes in the meteorological parameters may lead to a significant change of N and dN/dh (Ayantunji et al., 2011; Kablak, 2007; Priestley & Hill, 1985). When such changes occur, they impact the radio link and may lead to reduced performance, that is, increased error rate, reduced data rate, and reduced link availability, or even a total loss of the link. For

example, Norland (2006) reported the loss of radar coverage when important changes in the meteorological parameters occur while Serdega and Ivanovs (2007) reported a loss of microwave links with seasonal variations that change the refractive index.

Climate parameters vary from one season to another, and in some geographical locations, they can be very unstable (Pankauskas & Bukantis, 2006). There can be significant random variations year on year and may be cyclic variations or longer-term trends. Changes in the climatic parameters imply that the parameters N and dN/dh may vary.

According to research conducted by the Intergovernmental Group on Climate Change (L. Gagno, 2000; Roy, 2014; Watson, 2001), the thermal regime and precipitation patterns could change significantly in the near future, in particular at high latitudes. During the last three decades, there has been an increasingly rapid evolution of CC. These changes are coupled with increasing probability of certain extreme events, like extreme and frequent droughts and floods, and storms of rare violence (Climate Trends and Variations Bulletin, 2018; L. Gagno, 2000; Ouranos, 2014). In this context, more and more scientific research has been dedicated to the influence of this change on various aspects of life (L. Gagno, 2000). According to (Lemmen & Warren, 2004), in a few years, the effects of CC will be observed in coastal areas of northern regions in the form of a modification of the Canadian landscape and conversion of natural habitats (L. Gagno, 2000).

Some research has shown an increase in a 1.6 °C increase in the mean annual temperature in Canada over the period 1948 to 2010. According to these studies, this temperature increase is particularly due to higher and higher temperatures in winter and spring. Although this trend is observed in the entire Canadian territory, it is observed particularly in the Far North and regions located in high latitudes ("Climate Trends and Variations Bulletin," 2018). These new climatic conditions are likely to significantly affect the evolution of climate parameters and hence the atmospheric refractivity and may, therefore, affect the communication grid.

Considering the above mentioned, a study was proposed for the Canadian environment of climate data at Kuujuaq station located in northeastern Quebec. The Kuujjuaq station is in the Arctic area. The climate of the Arctic is characterized by long, cold winters and short, relatively warm summers. Precipitation occurs mainly as snow, and the average of the observed rainfall is low with an average of 400 mm in the year. Winter temperatures range from −50 to 0 °C, while the average summer temperatures fall between −10 to 10 °C. (ANON, 2018; UNIKTOUR.COM, 2018).

Note that this is the first study for the Northern Quebec region, which is characterized by a cold climate throughout the year and precipitation is in the form of snow.

In the ITU-R Recommendations (Recommendations, I., 2017), the geoclimatic factor, K, is defined for a given location and climate. The percentage of time p_0 at which deep, clear-air multipath fading is observed increases in direct proportion to K. The K factor, in turn, depends on the surface refractivity gradient not exceeded for 1% of an average year (see equation (12)).

There are two approaches to obtain the refractivity profile. One approach consists of using radiosonde data measured at different times of the day at various heights (Falodun & Ajewole, 2006). The second approach consists of measuring the meteorological parameters at different times of the day at the surface and then using some empirical formulas to estimate these parameters at a given height. In this paper, as we will see in section 3, the second approach is used. The geoclimatic factor, K, required for the design of microwave links may then be found.

Note that in cases where local data are not available, ITU tables provide estimated values of the radio refractivity and its gradient and also the geoclimatic factor (Canada, 2018; Climate Trends and Variations Bulletin). However, it is recommended to consider local meteorological parameters for a given geographical location, since as we will see later in this paper and in already published papers, the values provided by the ITU maps can be significantly different from the actual local data. ITU-R models are predicated on the assumption of fixed, long-term values for climate parameters.

To the best of our knowledge, in the literature, the temporal variability due to CC is not considered although as shown in Agba et al. (2013), CCs can have a significant impact on radio propagation. Thus, the meteorological parameters are subject not only to seasonal variations but also to a temporal evolution (from one year to another; Agba & Ali, 2012; Agba et al., 2011).

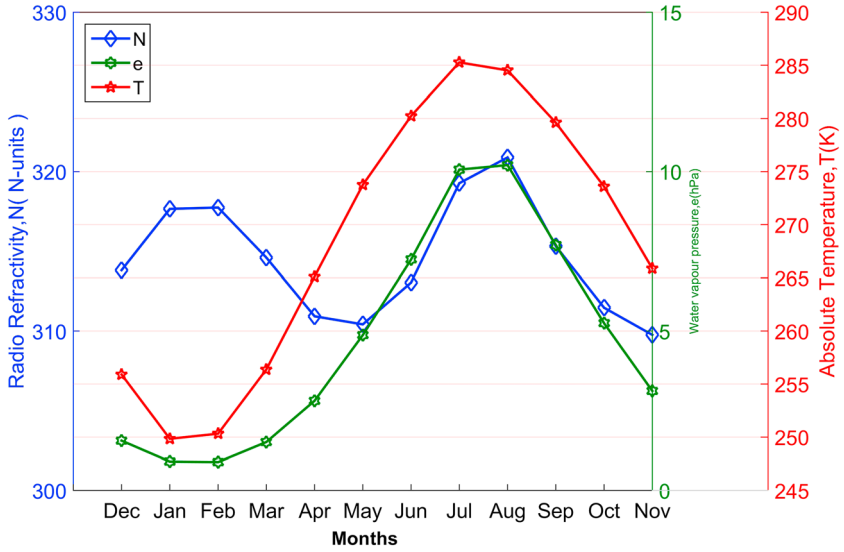

Figure 1. Mean monthly variations of N_s (1979 to 2013).

The main contribution of this paper is to consider both the seasonal variation and the temporal evolution of the meteorological parameters year on year and analyze their impact on the above-mentioned indices used during the design of the microwave link in arctic regions. This is achieved by using long-term (35 years) measured meteorological data in the Kuujuaq station (Quebec, Canada).

The rest of the paper is organized as follows. Section 2 provides a theoretical background. In this section, the formulas used to estimate the refractivity gradient, the refractivity, and the temperature, pressure, and water vapor at a given height are described. In section 3, the obtained results are analyzed, and some recommendations are given based on this analysis. Section 4 highlights the conclusions.

2. Theoretical Background

The vertical refractivity gradient in the lowest part of the troposphere, immediately above the ground surface, is used for the assessment of ray curvature, ducting, and multipath on terrestrial line-of-sight links. The occurrence of these phenomena depends essentially on the pressure, temperature, and relative humidity of the air. In the analysis, the troposphere is viewed as a dielectric medium. Its refractive index, denoted here by n, is determined by (Sizun & de Fornel, 2005):

$$n = \sqrt{\varepsilon_r \mu_r}, \tag{1}$$

where ε_r is the relative permittivity and μ_r is the relative permeability. The index n has a mean value around 1.0003, and variations of n at ground level are very low ($\pm 10^{-5}$). However, these small variations cause radio waves to bend significantly over paths of several kilometers and must be considered. For this reason, another index called refractivity and denoted here by N is used instead of n. These two indices are related by the following relationship (Recommendation, I, 2017b; Sizun & de Fornel, 2005):

$$n = 1 + N \times 10^{-6}. \tag{2}$$

The surface refractivity gradient dN/dh, which for convenience we denote dN_1, is determined by the following formula (AbouAlmal et al., 2013; Abu-Almal & Al-Ansari, 2010):

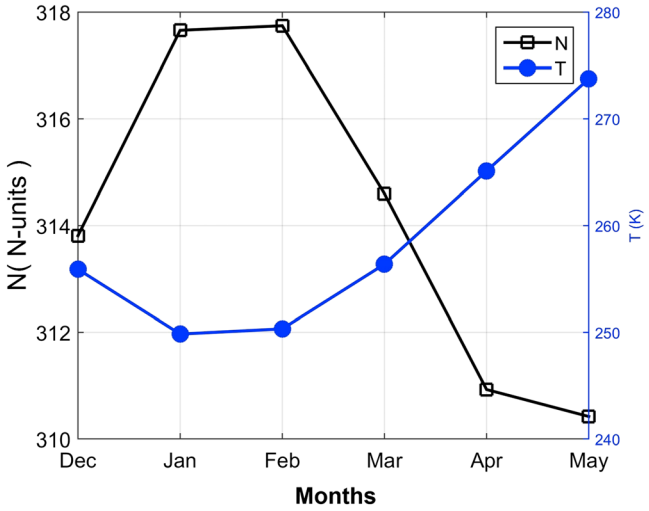

Figure 2. Mean monthly variations of N in the first cycle.

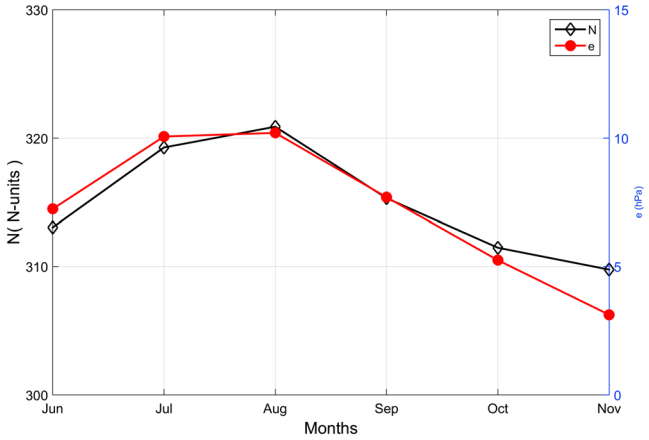

Figure 3. Mean monthly variations of N in the second cycle.

$$dN_1 = \frac{(N_2 - N_1)}{(h_2 - h_1)}, \tag{3}$$

where N_1 and N_2 are the refractivity values at heights h_1 and h_2, respectively. In this paper we consider $h_2 = 65$ m and $h_1 = 0$ m.

The refractivity can be determined either by measuring it directly with a refractometer or by calculating it from meteorological data. Equation (3) shows a need to determine the refractivity at a given height. Therefore, the following equation is used to determine the refractivity at height h (Recommendation, I., 2017b):

$$N(h) = \frac{77.6}{T(h)}\left(P(h) + 4810\frac{e(h)}{T(h)}\right), \tag{4}$$

where $P(h)$ is the total atmospheric pressure in hectopascals, $e(h)$ is the water vapor pressure in hectopascals, and $T(h)$ is the absolute temperature in Kelvin at height h in kilometers. The water vapor pressure in hectopascals is determined by (Recommendation, I., 2017b):

$$e(h) = \frac{\rho(h).T(h)}{216.7}, \tag{5}$$

where $\rho(h)$ is the water vapor density in grams per cubic meter. It is determined as (Recommendation, I, 2017a):

$$\rho(h) = \rho_s e^{-\frac{h}{2}}, \tag{6}$$

where ρ_s is the water vapor density at the surface. There are several methods to determine ρ_s. In this paper the following formulae have been used (Liebe, 1987):

$$\rho_s = \frac{H_s\theta^6}{5.752}10^{(10-9.834\theta)}, \tag{7}$$

where $\theta = 300/T_S$ and H_S and T_S are the relative humidity and the absolute temperature in Kelvin at the surface, respectively. The relative humidity $H(h)$ in percent at a given height, h, is (Recommendation, I, 2017b):

$$H(h) = 100\frac{e(h)}{e_s(h)}, \tag{8}$$

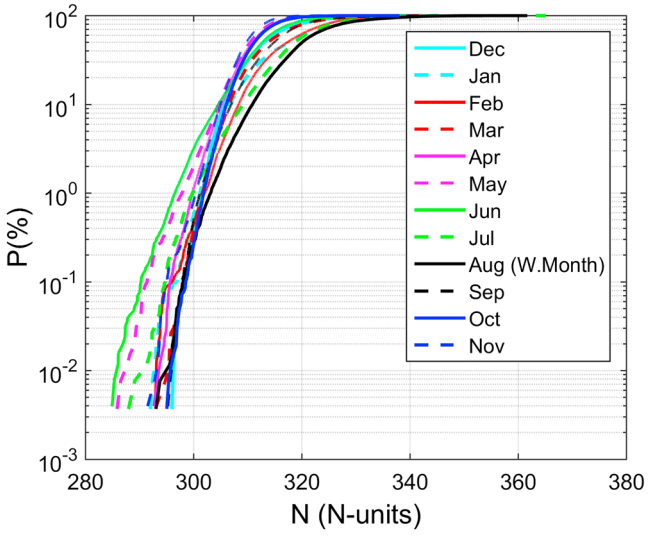

Figure 4. Monthly cumulative distributions of N (1979–2013).

where $e_s(h)$ is determined according to Jonhsnhweather (2018) by

$$e_s(h) = 6.11\times10^{\frac{7.5t(h)}{237.7+t(h)}}, \tag{9}$$

where $t(h)$ is the temperature $T(h)$ converted to degrees Celsius. The values of $T(h)$ and $P(h)$ are determined according to the recommendation ITU-R P.835-6 using the following formula (Recommendation, I, 2017a):

$$T(h) = T_s - 6.5h. \tag{10}$$

The following formula is used to determine the total atmospheric pressure $P(h)$ at a given height, h (Recommendation, I, 2017a), where P_S is the pressure in hectopascals at the surface.

$$P(h) = P_s[T_s/(T_s - 6.5h)]^{-5.2558} \tag{11}$$

In equations (10) and (11) the variable h is the height in kilometers above the surface.

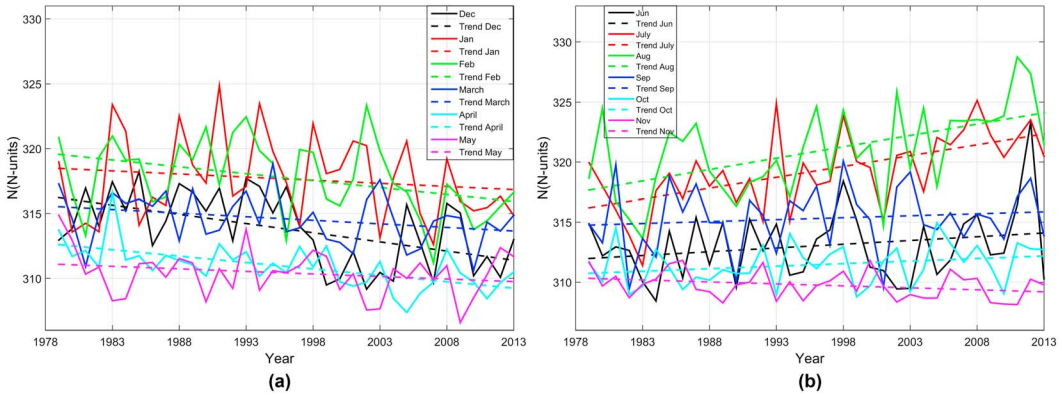

Figure 5. (a) Monthly long-term evolution of N; (b) monthly long-term evolution of N.

The geoclimatic factor, K, is an important design parameter. This factor is determined by (Recommendations, I., 2017)

$$K = 10^{-4.6-0.0027dN_1}. \tag{12}$$

The outage probability, P_w, is related to the geoclimatic factor as in Recommendations, I. (2017),

$$P_w = Kd^{3.1}\left(1+|\varepsilon_p|\right)^{-1.29} f^{0.8}\left(10^{-0.00089h_L - A/10}\right), \tag{13}$$

where f is the frequency (gigahertz); A is the fade depth (decibel), and $|\varepsilon_p|$ is the magnitude of the path (milliradian):

$$|\varepsilon_p| = \frac{|h_r - h_e|}{d}, \tag{14}$$

where h_r and h_e are the antenna heights (meters) and d is the path length (kilometers).

In summary, a procedure that consists of the following main steps is used to estimate dN_1:

1. N_1 is the same as the surface refractivity (Ns). It is estimated according to equation (4) by setting $h = 0$.
2. The refractivity, N_2 at height 65 m is estimated according to equation (4) by setting $h = 65$ m.
3. The vertical refractivity gradient, dN_1, is calculated according to equation (3).

Table 1
Correlation Between Monthly Values of N and Water Vapor and Correlation Between Monthly Values of N and Temperature

	Correlation coefficient (ρ)	
Month	Water vapor	Temperature
December	-0.64	-0.81
January	-0.75	-0.90
February	-0.71	-0.84
March	-0.63	-0.75
April	-0.25	-0.49
May	0.54	0.16
June	0.77	0.41
July	0.95	0.70
August	0.95	0.59
September	0.92	0.62
October	0.77	0.52
November	-0.05	-0.27

3. Results and Analysis

The meteorological data used in this paper were obtained from the Kuujuaq station. This station is situated on the northeastern part of Quebec, and it is located at 58.1° latitude and −68.42° longitude, with an altitude of 39.9 m above mean sea level.

From the Kuujuaq station local radiosonde meteorological data are not available. Only local climatic data such as temperature, dew point temperature, relative humidity, and pressure, at the surface, are available. These climatic parameters can be found at the Canada Environment site in the form of *csv* or *xml* files (Canada, 2018). In this paper for further analysis, we converted these files to Excel files.

For the sake of this analysis, the year runs from December to the following November. For example, the year labeled as 2013 runs from December 2012 to November 2013.

Table 2
Monthly Mean Surface Refractivity (N Units)

N	Min	Max	Mean	ITU	Linear best fit
N_{Feb}	311.2	323.3	317.7	320	-0.1064x + 316.3603
N_{Aug}	313.7	328.7	320.9	320	0.1894x + 317.4819

For the sake of simplicity, analyses of the obtained results are divided into three types, which are detailed in subsections 3.1 and 3.2 below, covering surface refractivity and refractivity gradient, respectively.

3.1. Analysis of the Surface Refractivity

The mean monthly ($N_{\text{mean 35 years}}$) variation of surface refractivity, N_s, averaged over the analyzed period of 35 years is shown in Figure 1.

Figure 1 shows that while temperature and humidity have an annual cycle with minima around January–February and maxima around July–August, N_s has two cycles per year. This occurs because, as seen in equation (4), N_s has a strong "dry" and a weak "wet" component. The "dry" component proportional to P/T varies inversely with temperature. The wet component varying with e/T^2 is dominated by the humidity variation and is thus "in-phase" with the temperature cycle. When these components are added, the January–February peak reflects a high dry component while the somewhat higher July-August peak reflects the high wet component.

The period from December to May (see Figure 2) belongs to the first cycle of N. In this cycle, we found a high inverse correlation ($\rho = -0.944$) between the evolution of N and variation of the temperature. The period from June to November (see Figure 3) belongs to the second cycle of N. In this cycle, we found a high correlation ($\rho = 0.962$) between the evolution of N and variation of water vapor.

Figure 4 shows the cumulative distributions of N for all months. For a percentage of time less than 1%, the worst months (months with highest values of N) are December, October, September, and March. For all remaining time percentages, the worst month is August.

Figure 5 shows the monthly variations of N and their corresponding trends for all 12 months for the analyzed period.

As seen in Figure 5a, the monthly average values of the surface refractivity decrease from year to year over the period from December 1978 to May 2013. The highest decrease of the N is observed for the month of December and the lowest one for the month of May. In these months the outage probability P_w will be lower from year to year. Figure 5-b shows that the monthly average values of the surface refractivity increase from year to year over the period from June 1978 to October 2013. The highest increase of the N is observed for the month of August and the lowest one for the month of October. For the month of November, a slow decrease of N is observed.

The obtained values of the correlation coefficient (ρ) between the mean monthly values of N and water vapor as well as temperature are shown in Table 1.

The values of the correlation coefficient shown in Table 1 indicate that the evolution of N depends on both water vapor and temperature.

From Table 1 the following can be observed:

1. The months of December, January, February, and March have a high inverse correlation with temperature.
2. The months of June, July, August, September, and October have a high correlation with water vapor pressure.
3. The month of May is characterized by a medium correlation with humidity and a weak correlation with temperature.
4. The month of November is characterized by a very weak inverse correlation with humidity and a weak correlation with temperature.

Table 3
Trend of Monthly Mean Temperature and Water Vapor Pressure

	Linear best fit	
Parameter	February	August
Temperature, K	0.1012x + 248.0063	0.0537x + 283.5524
Water vapor pressure, hPa	0.0056x + 0.7857	0.06x + 9.1263

Let us analyze the evolution of N in detail for the months of February and August. From Table 1 it is clear that there is a significant inverse correlation between the values of the refractivity and water vapor, as well as temperature for February. However, the temperature had more contribution because as one can see from Figure 2, February lies in the first cycle of the evolution of N where the value of N is mainly determined by the temperature. Table 1 shows a high correlation between N_{Aug} and water

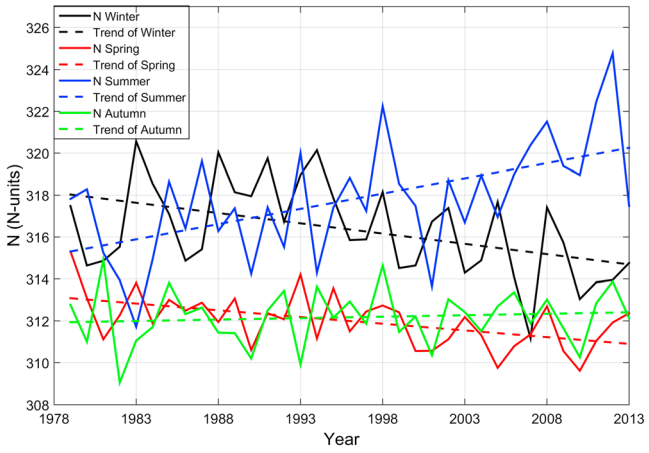

Figure 6. Seasonal variations of the mean surface refractivity (1979-2013).

vapor and a relatively weak correlation with temperature. However, the water vapor (humidity) had more contribution because as one can see from Figure 3 August lies in the second cycle of the evolution of N where the value of N is mainly determined by the humidity.

Observations of the mean monthly values of N for these months are shown in Table 2. Column "ITU" shows the values taken from the ITU maps. While the yearly mean over the 35-year period remains in good agreement with the ITU values, this disguises the fact that the mean values for the worst months of February and August are diverging increasingly year on year throughout this period.

In Table 2 and all subsequent tables the variable, x is the year number of the analyzed period, that is, $x = 1, 2, 3, \ldots 35$.

It has been noted that while the mean value over the 35-year period is close to the value given in the ITU maps, there is a distinct trend. N_{Feb} decreases year on year, while N_{Aug} increases. This is because the variation of humidity is significantly more important in August compared to February in comparison to temperature variations. Trends for temperature and humidity are shown in Table 3.

These results confirm that the change in humidity is the parameter that most influences the change of N (Sizun & de Fornel, 2005). The values of the refractivity from the ITU maps for February and August are constant values. This is because ITU recommendations do not consider the evolution of climatic parameters (humidity, temperature, and pressure) over time.

3.1.1. Seasonal Variation of the Mean Surface Refractivity

In this study, analysis of the seasonal variation is also provided. Including winter, spring, summer, and autumn. Variation of the seasonal mean surface refractivity and their linear trends are given in Figure 6.

For each year, the obtained results show that the values of N are mainly lower in spring and autumn seasons, and higher in the winter and summer seasons. From Figure 6, it can be observed that for summer and autumn seasons, the evolution of the mean surface refractivity increases from one year to another. However, this increase is more significant in summer. This is due to the high humidity in summer from one year to another during the analyzed period. For winter and spring seasons, the evolution of the mean surface refractivity decreases from one year to another. However, this decrease is more significant in winter. For the 35-year period, the linear trends of the seasonal surface refractivity are shown in Table 4 for the four seasons. To make the connection between the seasonal evolution of N and climate, the linear trend of the evolution of the temperature and water vapor pressure is also shown in Table 4.

Over a period of 35 years, there is an increase in all seasons of the temperature and water vapor pressure. However, the increase of the water vapor pressure is most important in summer following by autumn, spring, and winter. The obtained values of the correlation coefficient between the seasonal values of N and water vapor as well as temperature are shown in Table 5.

From Table 5, it was observed a high correlation between N and water vapor pressure ($\rho = 0.92$) for summer, and a medium correlation between N and temperature ($\rho = 0.71$) for autumn. There is also a correlation between N and temperature in these seasons. However, the effect of this correlation is largely compensated by the correlation between N and water vapor pressure. For this reason, an increase of N is observed in these seasons. Table 5 shows that there is high inverse correlation between N and temperature in the winter ($\rho = -0.89$) and a weak inverse correlation ($\rho = -0.33$) in spring. There is also an inverse correlation ($\rho = -0.77$) between N and water vapor pressure in the winter season. However, the effect of this correlation is largely compensated by the inverse correlation between N and temperature. For this reason, a decrease of N is observed in this season. There is no correlation between N and water vapor pressure in the spring season.

Table 4
Linear Trends of Seasonal Surface Refractivity, Temperature, and Water Vapor Pressure

	Linear best fit		
Season	Surface refractivity, N units	Temperature	Water vapor pressure
Winter	-0.0983x + 318.1304	0.1228x + 249,862	0.0103x + 0.9365
Spring	-0.0643x + 313.1506	0.1074x + 263,1418	0.0121x + 2.849
Summer	0.1456x +315.1616	0.086x + 281,8232	0.0566x + 8.1668
Autumn	0.0139x + 311.9241	0.080x + 271,5958	0.0228x + 4.9412

Table 5
Correlation Between Monthly Values of N and Water Vapor and Correlation Between Monthly Values of N and Temperature

	Correlation coefficient (ρ)	
Season	Water vapor	Temperature
Winter	-0.77	-0.89
Spring	-0.00	-0.33
Summer	0.92	0.62
Autumn	0.71	0.31

3.2. Analysis of the Refractivity Gradient

An important index used in the design procedure for microwave links is the refractivity gradient, dN_1. This index is calculated based on the values of the refractivity at two different heights above the ground surface (Zilinskas et al., 2012). Values of dN_1 outside of the normal range ($dN_1 = -40$ N Units/km) are referred to as anomalous refraction. Values in the range ($-157 < dN_1 < -41$ N Units/km) cause superrefraction, values ($dN_1 < -157$ N Units/km) cause trapping or ducting, and dN_1 -41 N Units/km cause subrefraction. Superrefraction and ducting can cause propagation well beyond the normal radio horizon, which has the potential to cause interference with nominally independent links. Subrefraction causes fading on the intended link. Large negative values of dN_1 are also associated with an increased probability of deep, clear-air multipath fading (AbouAlmal et al., 2013).

In this paper, there are only measured local meteorological data at the surface. However, to determine dN_1, we need the value of N at some height (at 65 m in this case). For this reason, we estimated the local meteorological data according to the methodology described in section 2 of this paper. This approach is not accurate. For example, some phenomena such as temperature inversion (an increase in temperature with height) cannot be considered. However, in normal atmospheric conditions, the estimated values of dN_1 can give an idea of the evolution of dN_1. Our analysis will be limited to yearly and monthly variations of the mean refractivity gradient.

3.2.1. Yearly Variation of the Mean Refractivity Gradient

The mean yearly variations of the refractivity gradient over the period of the 35 years and the corresponding linear trend are given in Figure 7.

Figure 7 shows that years 1982, 1990, 1992, 2001, and 2009 have the highest values of the dN_1. Moreover, one can see that the year 1982 is characterized by the highest value of dN_1. The lowest value of dN_1 lies in 2012 and 1998. From Figure 3, it can be noted that yearly mean values lie in the range $-67.62 < dN_1\text{-}mean < -62.97$ N Units/km. Thus, superrefraction is the norm for this region.

The linear trend line clearly shows a marked year-on-year decrease in the annual mean dN_1-*mean*. This is due to the increase in temperature and water vapor during this period.

Our analysis shows that there is a perfect inverse correlation between the mean yearly values of dN_1 and temperature ($\rho = -0.72$) and between the mean yearly values of dN_1 and water vapor ($\rho = -0.95$). These results show that the evolution of the mean yearly value of dN_1 depends on the temperature and water vapor.

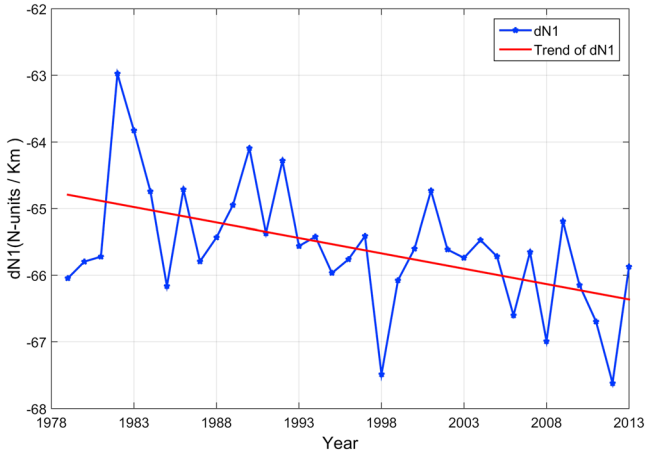

Figure 7. Mean yearly variations of the refractivity gradient at 0 and 65 m (1979 to 2013).

3.3. Monthly Variation of Mean the Refractivity Gradient

Figure 8 shows the mean monthly variations of the refractivity gradient $dN_{1\text{-mean-month}}$ over a period of 35 years.

From Figure 8, it can be observed that the shape of the dN_1 curve is inversely proportional to the temperature and water vapor curves. Also, for all the years, it was observed that the highest values are found in winter and the lowest in summer. The period from December to March corresponds to the period in which the climatic conditions are very difficult (very cold, precipitation in the form of snow, and wind storm). During this period, $dN_{1\text{-mean-month}}$ varies between limits that lead to the superrefraction phenomenon. The period from April to June and September to November is a relatively pleasant period of the year. In this period, the precipitations are in the form of rain. During this period the superrefraction phenomenon takes place. It can also be noted that the period from July to August is also a relatively pleasant period of the year. In this period the precipitations are in the form of rain. During this period, there is also a superrefraction phenomenon.

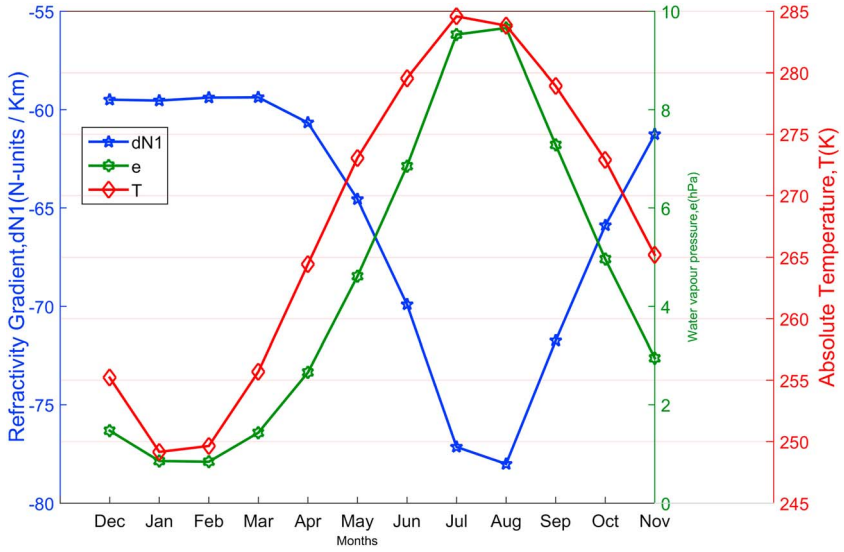

Figure 8. Mean monthly variations of refractivity gradient at 65 m (1979 to 2013).

From Figure 8 August has a more negative value of dN_1. So in this month the geoclimatic factor has the highest value, as shown in equation (12), and hence, P_w will be the highest value as shown in equation (13).

4. Conclusion

In this paper, an analysis of the refractivity over a period of 35 years in the Arctic regions has been presented. The evolution of N over the analyzed period was characterized by two cycles. In the first cycle (from December to May), the temperature variation was the parameter that mostly determines the evolution of N. In the second cycle (from June to November) humidity mostly determines the evolution of N. The pressure undergoes a small variation in both cycles, so this parameter has practically no effect in the variation of N.

The mean value of N for the worst month (August in this case) was varied between 311.716 and 324.763 N Units.

The results of the analysis showed that the linear trends of the yearly variations of N over the analyzed period increase from year to year in the summer and autumn seasons. This is probably caused by CC. Thus, in the future, it is necessary to consider the impact of CC in the design of communications links in the Arctic regions.

Note that for each year from 1979 to 2013 the mean of the refractivity gradient $dN_{1\text{mean}}$ varies between −67.62 and −62.97 N Units/km with standard deviation STD = 0.94. Since $-150 < dN_1\text{-mean} < -41$, the superrefraction phenomenon is predicted. The value of $dN_{1\text{-ITU}}$ determined for this station is $dN_{1\text{-ITU}} = -250$ N Units/km. For all years in this period, $dN_{1\text{-mean}}$ $dN_{1\text{-ITU}}$.

The superrefraction conditions for electromagnetic wave propagation predicted by the ITU maps have been observed.

The values of dN_1 were determined using the estimated values of local meteorological data at height 65 m. In the future, we hope that measured local meteorological data will be available at a different height. If this will be the case, we plan to use this data to determine dN_1 more accurately and analyze the evolution of the refractivity at different heights.

Acknowledgments
All measured data are available in the Google Drive website (https://drive.google.com/file/d/1tWaCcRLwxeDy8WFp8cvnXDI93BS3Higi/view?usp=sharing).

References

AbouAlmal, A., Abd-Alhameed, R. A., Al-Ansari, K., AlAhmad, H., See, C. H., Jones, S. M., & Noras, J. M. (2013). Statistical analysis of refractivity gradient and β_0 parameter in the Gulf Region. *IEEE Transactions on Antennas and Propagation*, *61*(12), 6250–6254. https://doi.org/10.1109/TAP.2013.2279999

Abu-Almal, A., & Al-Ansari, K. (2010). Calculation of effective Earth radius and point refractivity gradient in UAE. *International Journal of Antennas and Propagation*, *2010*, 1–4. https://doi.org/10.1155/2010/245070

Agba, B. L., & Ali, O. B. S. (2012). Experimental validation of ITU method for terrestrial line-of-sight links design. Paper presented at the Electrical & Computer Engineering (CCECE), 2012 25th IEEE Canadian Conference on.

Agba, B. L., Ben Sik Ali, O., &Bettouche, Y.(2013). Impact Des Changements Climatiques Sur L'ingénierie Des Communications Sans Fil – Cas Des Liaisons Hertziennes. Paper presented at the EIC Climate Change Technology Conference 2013 Montreal, Canada.

Agba, B. L., Ben-Sik-Ali, O., Morin, R., & Bergeron, G. (2011). Recent evolution of ITU method for prediction of multipath fading on terrestrial microwave links. Session 3P7 RF and Wireless Communication, Multipath, 857.

Ali, S., Malik, S. A., Alimgeer, K. S., Khan, S. A., & Ali, R. L. (2012). Statistical estimation of tropospheric radio refractivity derived from 10 years meteorological data. *Journal of Atmospheric and Solar-Terrestrial Physics*, *77*, 96–103. https://doi.org/10.1016/j.jastp.2011.12.001

ANON. (2018). ANON. Retrieved 06/04/2018, from http://geographie.chez-alice.fr/index_fichiers/theorie/Ch11_Climat/climats_canada.html

Ayantunji, B., Okeke, P., Urama, J., & Najib, Y. (2011). A semi-empirical model for vertical extrapolation of surface refractivity over Nigeria. The African Review of Physics, 6.

Canada, G. o. (2018, 12/01/2018). Local meteorological data from http://climat.meteo.gc.ca

Climate Trends and Variations Bulletin. (2018). Retrieved 05/05/2018, from https://www.canada.ca/en/environment-climate-change/services/climate-change/trends-variations.html

Falodun, S., & Ajewole, M. (2006). Radio refractive index in the lowest 100-m layer of the troposphere in Akure, South Western Nigeria. *Journal of Atmospheric and Solar-Terrestrial Physics*, *68*(2), 236–243. https://doi.org/10.1016/j.jastp.2005.10.002

Freeman, R. L. (2006). *Radio system design for telecommunication* (Vol. 98). Hoboken, NJ: John Wiley & Sons.

Guo, G., & Li, S. (2000). Study on the vertical profile of refractive index in the troposphere. *International Journal of Infrared and Millimeter Waves*, *21*(7), 1103–1111. https://doi.org/10.1023/A:1026452522574

Jonhsnhweather. (2018). Vapor pressure. Retrieved 22/01/2018, from http://www.johnsnhweather.com/formulas/vaporPressure.html

Kablak, N. (2007). Refractive index and atmospheric correction to the distance to the Earth's artificial satellites. *Kinematics and Physics of Celestial Bodies*, *23*(2), 84–88. https://doi.org/10.3103/S0884591307020079

L. Gagno, M. P. (2000). Changement Climatique la Performance d'Hydro-Quebec, 2000. Quebec, Canada.

Lemmen, D. S., & Warren, F. J. (2004). Climate change impacts and adaptation: A Canadian perspective.

Liebe, H. J. (1987). A contribution to modeling atmospheric millimeter-wave properties. *Frequenz*, *41*(1-2), 31–36.

Norland, R. (2006). Temporal variation of the refractive index in coastal waters. Paper presented at the Radar Symposium, 2006. IRS 2006. International.

Ouranos. (2014). Ouranos. from http://www.ouranos.ca/fr/synthese2014

Pankauskas, M., & Bukantis, A. (2006). The dynamics of the Baltic Sea Region climate humidity in 1950–2004. *Annales Geographicae*, *39*(1), 5–14.

Priestley, J., & Hill, R. (1985). Measuring high–frequency refractive index in the surface layer journal of atmospheric and oceanic technology, Vol. 2.

R-3670-2008, D (2009). Budget Des Investissements 2009. Retrieved 2/01/2018, from http://www.regie-energie.qc.ca/audiences/3670-08/Requete_3670-08/B-1_HQT-1Doc1_3670_29juil08.pdf

Recommendation, I (2017a). 835-6, "Reference standard atmospheres: ITU-R". Recommendations and Reports of the ITU-R

Recommendation, I (2017b). 453-13,"The radio refractive index: Its formula and refractivity data". Recommendations and Reports of the ITU-R.

Recommendations, I (2017). 530-17, "Propagation data and prediction methods required for the design of terrestrial line-of-sight systems". ITU-R.

R. Roy, J. C.-G., Élyse Fournier Et Claude Desjarlais. (2014). Synthèse Des Connaissances Sur Les Changements Climatiques 2014. Quebec, Canada.

Serdega, V., & Ivanovs, G. (2007). Refraction seasonal variation and that influence on to GHz range microwaves availability. *Elektronika ir Elektrotechnika*, *78*(6), 39–42. https://doi.org/10.5755/j01.eee.78.6.10812

Sizun, H., & de Fornel, P. (2005). *Radio wave propagation for telecommunication applications*. Berlin Heidelberg New York: Springer.

UNIKTOUR.COM. (2018). Climat Arctique

Watson, R. T. (2001). *Synthesis report: Contribution of Working Groups I, II, and III to the Third Assessment Report of the Intergovernmental Panel on Climate Change*. Cambridge: Cambridge University Press.

Zilinskas, M., Tamosiunaite, M., Tamosiuniene, M., Valma, E., & Tamosiunas, S. (2012). Gradient of radio refractivity in troposphere. Paper presented at the Progress In Electromagnetics Research Symposium Proceedings, Moscow, Russia, August.